Metrol. Meas. Syst., Vol. 30 (2023) No. 4, pp. 617–635
DOI: 10.24425/mms.2023.147957

PAN POLSKA AKADEMIA NAUK

METROLOGY AND MEASUREMENT SYSTEMS
Index 330930, ISSN 0860-8229
www.metrology.wat.edu.pl

M&MS

THE DEVELOPMENT OF A META-LEARNING CALIBRATION NETWORK FOR LOW-COST SENSORS ACROSS DOMAINS

Tianliang Feng[1)], Xingchuang Xiong[2)], Shangzhong Jin[1)]

1) College of Optical and Electronic Technology, China Jiliang University, Hangzhou, Zhejiang 310018, China (✉ *FengFengtl@outlook.com, jinsz@cjlu.edu.cn*)
2) National Institute of Metrology, Beijing 100029, China (*xiongxch@nim.ac.cn*)

Abstract

Low-cost sensor arrays are an economical and efficient solution for large-scale networked monitoring of atmospheric pollutants. These sensors need to be calibrated in situ before use, and existing data-driven calibration models have been widely used, but require large amounts of co-location data with reference stations for training, while performing poorly across domains. To address this problem, a meta-learning-based calibration network for air sensors is proposed, which has been tested on ozone datasets. The tests have proved that it outperforms five other conventional methods in important metrics such as mean absolute error, root mean square error and correlation coefficient. Taking Manlleu and Tona as the source domain and Vic as the target domain, the proposed method reduces MAE and RMSE by 17.06% and 6.71% on average, and improves R2 by an average of 4.21%, compared with the suboptimal pre-trained multi-source transfer calibration. The method can provide a new idea and direction to solve the problem of cross-domain and reliance on a large amount of co-location data in the calibration of sensors.

Keywords: low-cost sensor array, ozone pollutants, timing characteristics, meta-learning algorithm, calibration.

1. Introduction

Urban air pollution notably impacts the quality of life and overall public health. Contaminants such as *particulate matter* (PM), ozone (O_3), carbon monoxide (CO), and nitrogen dioxide (NO_2) are capable of provoking ailments associated with both the respiratory and cardiovascular systems. According to the World Health Organization (WHO), over 4.2 million deaths occur annually due to air pollution [1]. In order to enhance the monitoring and control of air pollution, governments and related entities have deployed high-precision reference stations in critical areas, but rising costs and high maintenance have prevented intensive deployment. In recent years, *low-cost sensor arrays* (LCSAs), consisting of low-cost target pollutants sensors and other sensors such as temperature, humidity [2–5] and other gases that are cross-sensitive to the target pollutants [4–6], have been applied in urban concentration monitoring due to their low price, removability and maintenance-free characteristics [7–10].

Article history: received April 4, 2023; revised July 28, 2023; accepted August 9, 2023; available online November 18, 2023.

Given the potential drift in measurement outcomes induced by environmental shifts and intrinsic sensor aging following the deployment of the LCSA [11, 12], the accuracy and reliability of measurement data may be compromised. Thus, post-calibration becomes decidedly critical [13, 14]. Post-calibration refers to the calibration process undertaken after sensor deployment, devised to eliminate error sources that could destabilize sensor performance in actual deployment environments, thereby augmenting the measurement precision and data quality of the LCSA. The calibration models currently use a variety of methods ranging from simple statistical learning methods [15–19] to complex deep learning techniques [20–23], from a "one-to-one" approach where the measured values at the current moment are input to output the calibrated values at that moment, to a "many-to-many" approach where the measured values at a set of consecutive moments are input to output the calibrated values at the corresponding moment [20]. Most calibration models require the LCSA to be co-located with a reference station for a long period of time to obtain sufficient data for training [23] and to adapt to current patterns of environmental pollutant change. In practice, however, complex models with weak generalization capabilities can degrade or even become unusable when the LCSA crosses the domain into a new environment, at which point the LCSA needs to be co-located with a reference station within this new setting for a long period of time and the model retrained using the new data. Even some areas have problems such as low sampling frequency of reference stations or restricted access to reference station data. This results in the calibration model of LCSA in that area not learning the optimal parameters, thus affecting measurement accuracy.

Recent studies have addressed the problem above by transfer calibration, and papers [22,24,25] have applied transfer calibration to map raw feature data collected by low-cost $PM_{2.5}$ sensor arrays in the source and target domains in high dimensions, allowing the target domain sensor arrays to be calibrated with the help of readings from reference stations in the source domain, but this approach requires sensors to collect raw data in the target domain for a sufficient length of time to achieve this. Methods [23, 26, 27] include the use of source domain data to generate a pre-trained model and a small amount of data in the target domain to fine-tune the model parameters to form a calibration model with high accuracy in the target domain. However, the calibration model used does not capture the dynamic patterns of pollutants over time, and most gaseous pollutants demonstrate periodicity, thus this method is not the best choice for calibrating LCSA.

In light of this, we have devised a calibration method: initially proposing a temporal LCSA calibration model – an *air sensor calibration network* (ASCN). Subsequently, in conjunction with the *model-agnostic meta-learning* (MAML), we formed ASCN-MAML. This method ultimately solves the cross-domain problem in LCSA calibration models and the scarcity of target domain data. In paper [24], the authors propose a hypothesis that when the distance between the source domain and the target domain is sufficiently close, the distribution of the actual concentration of pollutants in both locations is similar over a certain period. Based on this assumption, an *in-field calibration transfer* (ICT) method is proposed, mapping the data collected by the LCSA in the target domain and source domain, thereby enabling the LCSA of the target domain to be calibrated with the help of the reference station in the source domain. However, this method requires the LCSA to be placed in the target domain for a period of time to collect sufficient measurement data. The method proposed in this paper, ASCN-MAML, utilizes a meta-learner generated from co-location data in the source domain, and only needs to utilize a small amount of co-location data in the target domain to allow the meta-learner to quickly converge, creating a calibration model adapted to the target domain, thus enabling the LCSA to be rapidly deployed in the target domain. In paper [23], the authors proposed a low-cost $PM_{2.5}$ calibration method based on domain adaptation. This method uses a *deep neural network* (DNN) as the basic model, creates a pre-trained model with co-location data from the source domain and fine-tunes the

model with a small amount of co-location data from the target domain. The quickly generated calibration model performs reasonably well in the target domain. However, the basic DNN model used by the authors is a simple one-to-one model that does not consider the temporal changes in pollutant concentration. The basic ASCN model used in this paper employs a self-attention mechanism, capturing the dynamic patterns of pollutant concentration over time, thus offering performance superior to the DNN. In addition, the multi-source transfer calibration method with pre-training and fine-tuning used in this paper generates a pre-training model in which parameters are optimized in the source domain. This paper, aided by the special mechanism of MAML, uses a meta-learner generated from co-location data from multiple source domains, which takes into account the entire domain, including the optimal initial parameters of the target domain, and allowing the model to quickly adapt to the target domain while maintaining superior measurement accuracy.

1. ASCN introduces past and future measurements to capture the dynamic pattern of gas concentration changes over time, providing higher accuracy than conventional models.
2. ASCN uses meta-learning MAML training to solve the problem of poor ASCN performance across domains, and has higher accuracy compared to existing pre-training-fine-tuning based migration calibration methods.
3. The method significantly reduces the training cost of the model in the target domain by leveraging the source domain data, and the model is able to converge quickly with only a small amount of data in the target domain, which is more advantageous than conventional methods when faced with scenarios where co-location data is insufficient due to restricted access to reference station data, *etc*.

2. Design of methods

2.1. Summary

As shown in Fig. 1, the method consists of two phases. In the meta-learner training stage, continuous-time data is extracted from each source domain to generate a meta-learner with an

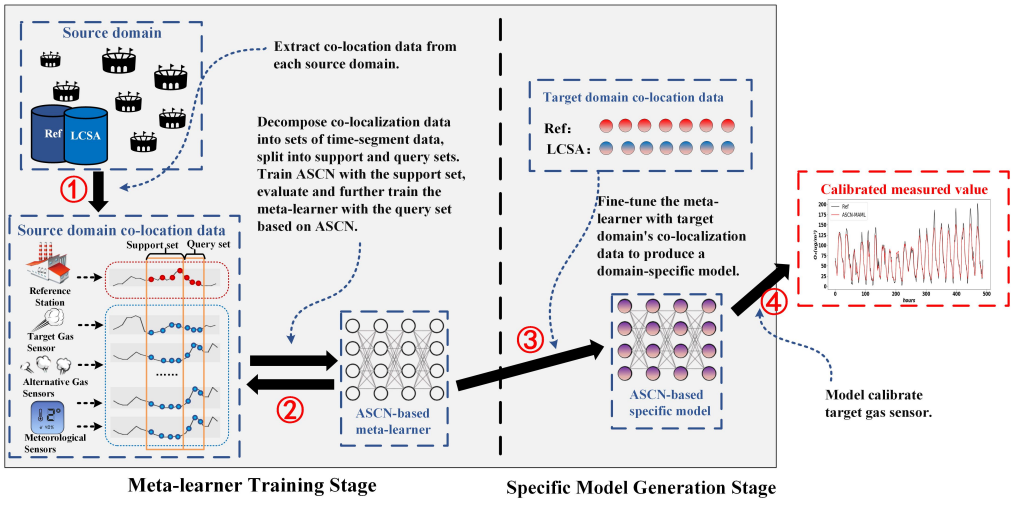

Fig. 1. ML calibration method flow: co-location data extraction, ASCN-MAML meta-learner generation, target domain model training, and sensor calibration.

ASCN as the base model in a MAML training method, which carries optimal parameters that can be quickly adapted to the target domain. In the specific model generation stage, the meta-learner is fine-tuned using a small amount of co-location data from the target domain to generate a specific ASCN available in that target domain, which is used to calibrate the LCSA readings in the target domain at subsequent times.

This section then briefly describes the network structure of the ASCN calibration model and focuses on the role of its key modules and the MAML meta-learning algorithm.

2.2. ASCN

2.2.1. Model structure

Our proposed calibration model, the ASCN, is structured as shown in Fig. 2. ASCN takes the measurement values of LCSAs in the past, present, and future 2δ time steps, and constructs a continuous time series $X_\delta \in R^{2\delta \times d}$ as input. Here, X_δ represents the time series matrix of the input sensor array readings, 2δ represents the length of the input time series, and d represents the dimension of the original and derived features collected by a single sensor array. The model finally outputs the calibrated values $\hat{Y}_\delta \in R^{2\delta \times 1}$ of the target pollutant sensor at the corresponding time.

The main part of this network is the multi-headed self-attention module, which inspired us the successful applications of TransFormer [28] in natural language processing [29–31], time

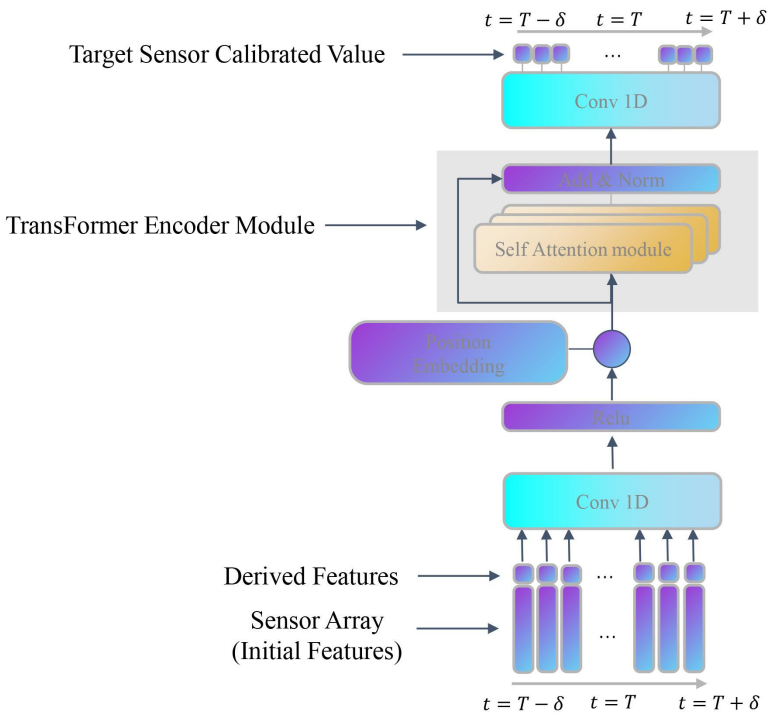

Fig. 2. ASCN calibration model: initial Conv1D and Relu for hidden representation, Position Embedding for relative position capture, Transformer Encoder for inter-temporal relationship learning, and final Conv1D for moment-specific calibration output.

series prediction [32, 33] and other fields. As the multi-headed self-attention module is more adept at handling complex inputs, the time series matrix $X_\delta \in R^{2\delta \times d}$ is first mapped to a hidden representation $U_\delta \in R^{2\delta \times s}$ by a 1D convolutional layer and a *rectified linear unit* (Relu) activation function before being input to the module, where s represents the hidden dimension. The Relu, is used to increase training speed, improve non-linearity, gradient propagation and reduce overfitting. The position embedding module adds a position matrix U^{pos} to the input which is used to capture the relative position of the LCSA acquisition data. The order of inputting to the LCSA acquisition data is important as it contains information about how the sensor readings change over time.

The multi-headed self-attention module is able to fully learn the hidden relationships between the readings taken by the LCSA at each moment in the input time series data and the readings taken by the sensor array at other moments in the series, with a single self-attention module represented as follows:

$$A_i = \text{Softmax}\left(\alpha Q_i K_i^T\right) V_i\,, \tag{1}$$

where $Q_i = W_i^q U$, $K_i = W_i^k U$, $V_i = W_i^v U$ are linearly transformed to the input by the weight matrix W_i^q, W_i^k, W_i^v respectively, $\alpha = \dfrac{1}{\sqrt{d}}$ denoting the scaling factor used to mitigate the product magnitude within a large number of matrices.

The entire TransFormer coding module is computed as follows: first the feature hiding matrix $U_\delta \in R^{2\delta \times s}$ is merged with the position matrix U^{pos} to form a new matrix U as input, after K self-attention modules, the residual connections are used to maintain the original information and prevent the gradient from disappearing, and finally the training process is stabilized by normalization to prevent overfitting. It is expressed by the mathematical expression as:

$$U = \text{concat}\left(U_\delta;\, U^{\text{pos}}\right), \tag{2}$$

$$U_k = BN\left(MSK_k(U) + U\right), \qquad k = 1, 2, \ldots, K. \tag{3}$$

The output U_k, $k = 1, 2, \ldots, K$ of the TransFormer coding module is used as input to the 1D convolutional layer, which outputs the calibration values $\hat{Y}_\delta \in R^{2\delta \times 1}$ of the target gas sensor in the LCSA.

2.2.2. Loss function

Our task is to solve the multiple output regression problem, the choice of loss function is a current hot research content, the commonly used loss function is the mean square error, Eq:

$$L_{\text{MSE}} = \frac{1}{2\delta} \sum_{i}^{2\delta} \left(Y_i - \hat{Y}_i\right)^2. \tag{4}$$

However, in practical application scenarios, the calibrated value of the output of the model after using L_{MSE} does not correctly capture the dynamic shape of the true pollutants value over the time series, so this paper introduces a shape and time loss function L_{DILATE} [34]. In summary, the loss function used in this paper is formulated as:

$$L = \lambda L_{\text{MSE}} + \mu L_{\text{DILATE}}, \tag{5}$$

where λ and μ are used to balance the constants of the two loss functions. L_{DILATE} in (5) is defined as:

$$L_{\text{DILATE}} = \omega L_{\text{shape}} + (1 - \omega) L_{\text{temporal}}\,. \tag{6}$$

In the equation, L_{shape} represents the shape-based loss function, while L_{temporal} stands for the time-based loss function, both of which are predicated upon the *dynamic time warping* (DTW) algorithm. ω is the weighting factor that orchestrates the relative significance of shape and temporal aspects. L_{DILATE} proves notably instrumental in addressing time series prediction issues as it explicitly disassembles the penalties affiliated with errors in shape and temporal alignment. This implies that the loss function dissects the loss into two distinct components: one concerning shape misalignment, and the other relating to temporal discrepancies, thereby facilitating a more precise and accurate prediction of abrupt fluctuations in non-stationary signals. The shape component penalizes inaccuracies in the prediction of the signal's shape. In contrast, the temporal component penalizes timing errors in the predicted changes. More exhaustive details concerning this loss function can be procured from the indicated literature [34].

2.3. Meta-learning algorithms

Model-agnostic meta-learning (MAML) algorithms [35] have been applied to a variety of problems, including few-shot learning, multi-task learning and reinforcement learning [36]. MAML trains a meta-learner with strong generalization capabilities based on source domain data, and learns from only a small amount of data in the target domain, achieving a high level of performance of the model in the target domain in a small number of iterations.

The basic model ASCN, based on the MAML training approach, uses data from multiple source domains to train a meta-learner $M_{\text{meta}}^{\text{ASCN}}$ with initialization parameters that converge quickly in the target domain for different environments and pollutant concentrations followed by a small number of data pairs in the target domain where there is a shortage of data to fine-tune the model $M_{\text{meta}}^{\text{ASCN}}$ to a specific model $M_{\text{fine-tune}}^{\text{ASCN}}$ that can be adapted to a particular target domain, as follows:

Training the meta-learner $M_{\text{meta}}^{\text{ASCN}}$ on the source domain: First, a random initialization $M_{\text{meta}}^{\text{ASCN}}$ is done to extract a continuous segment of data pi from the source domain and divide it into a support set $D_{\text{source}}^{S_{pi}}$ and a query set $D_{\text{source}}^{Q_{pi}}$. $D_{\text{source}}^{S_{pi}}$ is used to train the ASCN, while $D_{\text{source}}^{Q_{pi}}$ is used to evaluate the performance of ASCN and train $M_{\text{meta}}^{\text{ASCN}}$.

The gradient update formula used to train the ASCN is

$$\theta_{pi} \leftarrow \theta_{pi} - \alpha \nabla_{\theta_{pi}} L_{D_{\text{source}}^{S_{pi}}} \left(\theta_{pi}\right). \tag{7}$$

Here, α is the learning rate. The loss function is defined in (5)

For training the meta-learner $M_{\text{meta}}^{\text{ASCN}}$ with different time periods of query set $D_{\text{source}}^{Q_{pi}}$, and updating the parameters φ in the $M_{\text{meta}}^{\text{ASCN}}$, the equation is

$$\varphi \leftarrow \varphi - \beta \sum_{i} \nabla_{\varphi} L_{D_{\text{source}}^{Q_{pi}}} \left(\theta_{pi}\right). \tag{8}$$

Here, β is the learning rate. The loss function is used in (5).

The final meta-learner$M_{\text{meta}}^{\text{ASCN}}$ is saved and the specific ASCNs trained by the different support sets $D_{\text{source}}^{Q_{pi}}$ are discarded.

To train a specific model $M_{\text{fine-tune}}^{\text{ASCN}}$ to fit the target domain by using the target domain, we first train the model using the parameters φ in the initialization and a small amount of data from the target domain, update the φ again and finally test the performance using the subsequent data from the target domain.

The pseudo-code for the computation process is presented in Algorithm 1.

Algorithm 1 Calibration Method Based on MAML.

Requirement: D_{source}: source domain dataset; D_{target}: target domain dataset.

Requirement: α, β: learning rate

Randomly initialize parameters φ
while not done **do**
Randomly extracting multiple sets of data pi from multiple source domains D_{source}
for each data pi **do**
pi's front portion of data as support set $D_{\text{source}}^{S_{pi}}$, and the remaining data as query set $D_{\text{source}}^{Q_{pi}}$
Compute $\nabla_{\theta_{pi}} L_{D_{\text{source}}^{S_{pi}}}(\theta_{pi})$
Gradient update $\theta_{pi} \leftarrow \theta_{pi} - \alpha \nabla_{\theta_{pi}} L_{D_{\text{source}}^{S_{pi}}}(\theta_{pi})$
Evaluate $L_{D_{\text{source}}^{Q_{pi}}}(\theta_{pi})$
end for
Gradient update $\varphi \leftarrow \varphi - \beta \sum_i \nabla_{\varphi} L_{D_{\text{source}}^{Q_{pi}}}(\theta_{pi})$
end while
Initialize meta-learner $M_{\text{meta}}^{\text{ASCN}}$ with φ
φ is updated using a small training set of D_{target} to generate the basic model $M_{\text{fine-tune}}^{\text{ASCN}}$
Test the performance of $M_{\text{fine-tune}}^{\text{ASCN}}$ using the remaining data in D_{target}

3. Tests and results

This section evaluates the proposed calibration method. A publicly available ozone dataset and several conventional methods are used to assess the effectiveness and accuracy of the methods in this paper.

3.1. Test dataset

The LCSA dataset used in this paper is from the European H2020 CAPTOR project [37], which aims to raise public awareness of ozone pollution's harmful effects and that of environmental protection. The project participants deployed three test beds in Italy, Spain and Australia. These nodes are called Captor and each node contains four SGX Sensortech MICS 2614 metal-oxide O_3 sensors, as well as one temperature and one relative humidity sensor, as shown in Fig. 3. Each Captor node is powered by an external power supply and connected to the Internet via Wi-Fi or 3G.

We used data from three of these devices, numbered C17013, C17016 and C17017, with data collected from 26 May 2017 to 4. October 2017, and from their high-cost ozone reference stations Manlleu, Tona and Vic [38], which were set up and maintained by the Government of Catalonia, with a sampling frequency of 1 hour. Figure 4 delineates the relative positioning of the reference station to the Captor nodes. Specifically, Captor nodes deployed across Spain are marked with blue icons and annotated with the respective node numbers. The sites of reference stations are designated with red icons. Data collection points integral to this study are also indicated, using a bold red font for clarity and emphasis. In Section 3.4, Table 2 provides a further layer of information, presenting the GPS coordinates for the ozone reference stations situated in Manlleu, Tona, and Vic. Different features in the dataset have different ranges of data values. Because calibration model accuracy and training efficiency are affected by the scale of the input data, we normalized the feature portion of the dataset through the MinMaxScaler function in Scikit-Learn.

Fig. 3. Photograph of the interior of the nodes of the Captor.

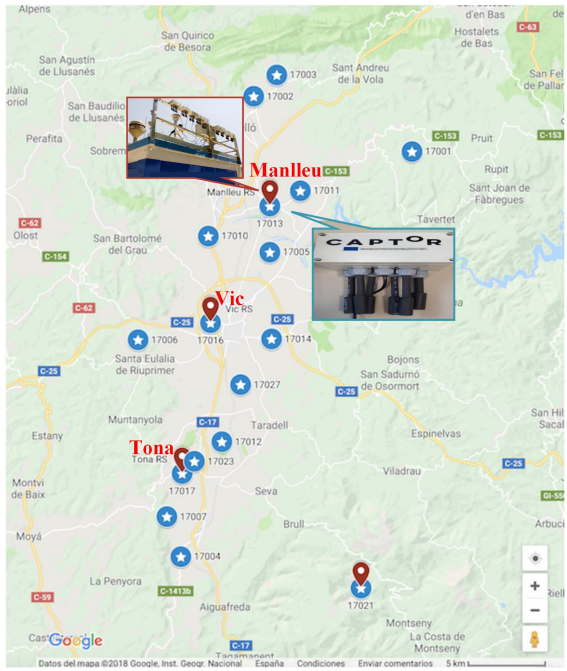

Fig. 4. Geographical layout of the Captor nodes: reference stations (red), Captor nodes (blue), with a label number adjacent to each node's mark.

3.2. Method comparison testing

A total of five comparison methods and one original method were used in this study, namely *uncalibrated* (UC), *target source train* (TT), *single source1 train* (SS1), *single source 2* train (SS2), *many source train* (MS), and *ASCN-MAML* (AM). UC denotes raw collected readings from the target contaminant sensors in the sensor array. In the dataset used, each sensor array contains four ozone sensors, and we took the average of the four readings as the raw readings

for that sensor array. TT denotes training of the ASCN model from scratch, using only a small amount of target-domain data that is available, without any pretraining. SS1 and SS2 indicate that the ASCNs were pre-trained with data sets from a single source domain respectively, and the resulting pre-trained models were fine-tuned using a small amount of data from the target domain. MS indicates that the ASCNs were pre-trained with data from all source domains and fine-tuned based on a small amount of data in the target domain. AM is the method proposed in this paper, see Section 2 for details.

3.3. Test parameter configuration

For both conventional methods mentioned in the paper and the proposed new method, the number of self-attention modules in the basic model ASCN is one, because this paper uses a structured dataset and too many self-attention modules will affect the meta-learner's convergence speed. The loss function (5) is partially set to. For this dataset, we set the timing length to $\lambda = 1$, $\mu = 0.15$. In the three conventional methods SS1, SS2, and MS, as detailed in Section 3.3, *adaptive moment estimation* (Adam) is used as the optimizer for the model ASCN. This model has a learning rate of 3E-4. In our method, the meta-learning phase trains the basic model using a stochastic gradient descent optimizer with a learning rate α = 1E-3; for the training meta-learner, Adam is used as the optimizer with a learning rate β = 1E-4, the support data in a single training session is the data from two days and the query set is the data from the following two days, and the iterations are not stopped until the losses in both the support and query sets have stabilized.

3.4. Result comparison

3.4.1. Verification of the ASCN Model

In light of the self-attention mechanism inherent within the ASCN model, it competes admirably with *recurrent neural network* (RNN) in temporal regression problems. Hence, prior to integrating ASCN as a foundational model with MAML, it is necessary to contrast ASCN with existing calibration models predicated on RNN modules to substantiate its effectiveness and accuracy. We carried out a performance comparison of the basic ASCN model with six prevalent methods where substantial co-localization data was accessible, in locations such as Vic, Tona, and Manlleu. The methods compared were:

1. UC: Uncalibrated raw ozone sensor readings, the average of measurements from four ozone sensors.
2. MLR: Multivariate linear regression, a typical sensor calibration method that linearly maps sensor readings to true values.
3. DNN: A straightforward, efficient deep learning model composed of three linear layers and activation functions, demonstrating exceptional performance in the sensor calibration field [23, 27]. The hidden units of the linear layer are set to 128.
4. LSTNet [39]: *Long short-term time series network* (LSTNet), combining convolutional neural networks, recurrent neural networks and autoregressive modules for multivariate time series prediction tasks. The input and output of this model were altered to apply it to our tasks, using parameters identical to the original paper.
5. DeepCM [22]: A calibration model based on RNN, utilizing past data during calibration. The parameters disclosed in the authors' paper were employed.
6. ASCN-G: A variant of ASCN, which eliminated the Position Embedding module and replaced the self-attention module with the *gated recurrent unit* (GRU) from RNN.

In this assessment, the dataset used was described in detail in Section 3.1. For deep learning models, we allocated 80%, 10%, and 10% of each location's dataset for training, validation, and testing, respectively. For the MLR method specifically, we used the first 90% and the last 10% as the training and testing sets, respectively. The results, as illustrated in Table 1, indicate that the UC method, being uncalibrated, is utterly unsuitable. MLR fails to consider the nonlinear relationship between low-cost sensors and true concentrations, resulting in lesser accuracy than subsequent models. Despite being a simple deep learning model, DNN excels with the dataset from Vic, outperforming even the time-series based models, although it did not meet expectations at the other two locations. LSTNet, DeepCM, and ASCN-G, all RNN-based temporal models, demonstrate similar performance in this assessment.

Table 1. Test results of the ASCN model and six post-deployment calibration algorithms at different locations.

Model	Loc1: Vic			Loc2: Tona			Loc3: Manlleu		
	MAE	RMSE	R^2	MAE	RMSE	R^2	MAE	RMSE	R^2
UC	72.62	91.82	–7.80	129.62	159.27	23.83	104.29	130.48	21.58
MLR	7.30	9.43	0.91	10.31	12.39	0.82	8.27	11.10	0.84
DNN	5.91	8.21	0.93	9.08	12.99	0.80	7.65	9.90	0.87
LSTNet	8.19	10.16	0.89	8.55	10.74	0.87	7.88	10.12	0.89
DeepCM	8.16	10.26	0.88	8.95	11.53	0.85	7.76	10.03	0.89
ASCN-G	6.03	8.30	0.93	8.86	11.27	0.85	8.11	10.54	0.87
ASCN	5.92	8.26	0.94	5.72	6.86	0.95	6.13	7.34	0.92

The ASCN method proposed herein proves to be the most effective in this evaluation. Averaging the results from the three locations, ASCN reduces the MAE by 27.82%, 28.55%, and 22.74% compared to LSTNet, DeepCM, and ASCN-G respectively. It also reduces the RMSE by 27.60%, 29.42%, and 25.41%, and improves R^2 by 6.04%, 7.25%, and 6.04%. This superior performance can be attributed to the self-attention mechanism within ASCN, which, compared to RNN, captures the complex patterns of ozone concentration over time, such as periodicity and trends, more flexibly. This mechanism can allocate different weights to each element within the input sequence, thereby enhancing performance when dealing with time series exhibiting complex patterns. Furthermore, both ASCN and ASCN-G introduce future measurements, thus producing more accurate calibration values than LSTNet and DeepCM.

3.4.2. Test Results

To evaluate the approach above, the following tests were conducted as shown in Table 1. We selected two locations as the source domain and the remaining one as the target domain. In order to ensure the integrity of the tests, three sets of tests were done, each with a different

Table 2. Data division and coordinates of the reference site.

Source domain	Target domain (Early/Mid peak)	Target domain GPS coordinates	
		Longitude	Latitude
Manlleu+Tona	Vic (5.27 – 6.17/7.15 – 8.15)	2°14′18.8″ E	41°56′08.4″ N
Manlleu+Vic	Tona (5.27 – 6.17/7.15 – 8.15)	2°13′14.7864″ E	41°50′49.7796″ N
Tona+Vic	Manlleu (5.27 – 6.17/8.1 – 8.31)	2°17′13.7868″ E	42°0′6.966″ N

source and target domain. In each set of tests, we selected data from the target domain during the early and mid-peak periods, assuming that ozone is a seasonal pollutant and the evnironment is usually more polluted with it during the summer months when meteorological factors such as high temperatures and high humidity accelerate ozone production and ozone concentrations fluctuate more than at the beginning of the peak.

We compared the proposed calibration algorithm with each of the other five basic methods. A small amount of data from the starting one to three days was used as training on the target domain dataset and the remaining data were used to test the calibration method and to assess the goodness of fit of the calibration method using three evaluation metrics: correlation coefficient (r-square, R2), *mean absolute error* (MAE), and *root mean squared error* (RMSE).

Table 3a. Metrics of various calibration methods evaluated over Vic as the target domain utilizing 1–3 days data from the early-phase of the ozone peak.

Method	1 day			2 days			3 days		
	MAE	RMSE	R^2	MAE	RMSE	R^2	MAE	RMSE	R^2
UC	62.96	83.53	–2.74	59.53	79.15	–2.31	55.83	73.05	–1.81
TT	69.64	81.65	–2.58	71.87	84.47	–2.53	67.01	79.32	–2.32
SS1	8.50	11.76	0.93	8.79	11.75	0.92	7.86	11.72	0.93
SS2	9.57	13.59	0.90	8.56	12.77	0.91	8.37	12.35	0.92
MS	7.41	10.89	0.94	8.66	12.74	0.92	8.12	12.52	0.94
AM	6.89	10.08	0.95	8.49	10.92	0.94	7.38	10.63	0.94

Table 3b. Metrics of various calibration methods evaluated over Vic as the target domain utilizing 1–3 days' data from the mid-phase of the ozone peak.

Method	1 day			2 days			3 days		
	MAE	RMSE	R^2	MAE	RMSE	R^2	MAE	RMSE	R^2
UC	91.00	117.94	–8.50	91.67	118.66	–8.82	89.16	114.64	–8.47
TT	62.29	72.54	–2.58	60.28	70.45	–2.45	60.06	70.08	–2.52
SS1	14.70	19.03	0.75	13.99	18.12	0.77	11.83	15.67	0.82
SS2	14.33	17.82	0.78	11.45	14.18	0.86	10.87	13.72	0.86
MS	12.45	15.61	0.83	10.95	13.79	0.87	10.81	13.83	0.86
AM	9.17	11.19	0.91	8.69	10.54	0.92	7.82	10.08	0.93

In Table 3a, we take Manlleu and Tona as the source domain, Vic is set as the target domain, and the test dataset time for the target domain is 5.27–6.17. When the time period is early summer in Vic, the beginning of the ozone peak, we assume that no more than three days of data are available at the reference station in the target domain during this time period, and the data for the remaining time period are used to test the performance of the different calibration methods and to observe the difference between the methods in obtaining a small amount of available training data in the target domain. As can be seen from the data in the table, in the case of the difference between the calibration values generated using the calibration methods on the subsequent test data and the true values, the results of the new AM method are better than those of the other five conventional methods. As ozone is a seasonal pollutant, we tested again during the midsummer period of 7.15–8.15 when ozone concentrations are high. This was to verify the effectiveness of the revised method. The results are shown in Table 3b. Still assuming no more than three days of actual data in the target domain, the calibrated method AM is still valid and highly accurate.

When analyzing the results for both time periods, the UC method performed the worst. This is because none of the four ozone sensors in the LCSA were laboratory calibrated. This resulted in significant differences between sensor readings and true values. The TT method was slightly better than the UC method, but still not usable because the basic model of ASCN contains a large number of parameters. Training with only a small amount of data does not make the model valid. The three SS1, SS2 and MS methods obtained more accurate model initialization parameters from single or multiple source domain data. The MS method is slightly more accurate than the SS1 and SS2 methods. Our proposed AM method showed superior performance due to the use of meta-learning to learn a generic calibration model in the source domain, which can better fit the data distribution in the target domain compared to other calibration methods.

Figure 5 presents a clear visual representation of the RMSE results derived from Table 3. Owing to the considerable discrepancy in RMSE values between the UC and TT methods and other approaches, these are excluded from the figure. The left and right plots illustrate the test results for the early and middle stages of the ozone peak in the target domain for Vic, respectively. The SS1 and SS2 methods are designated by blue and red lines, the MS method by a green line, and the AM method by a purple line.

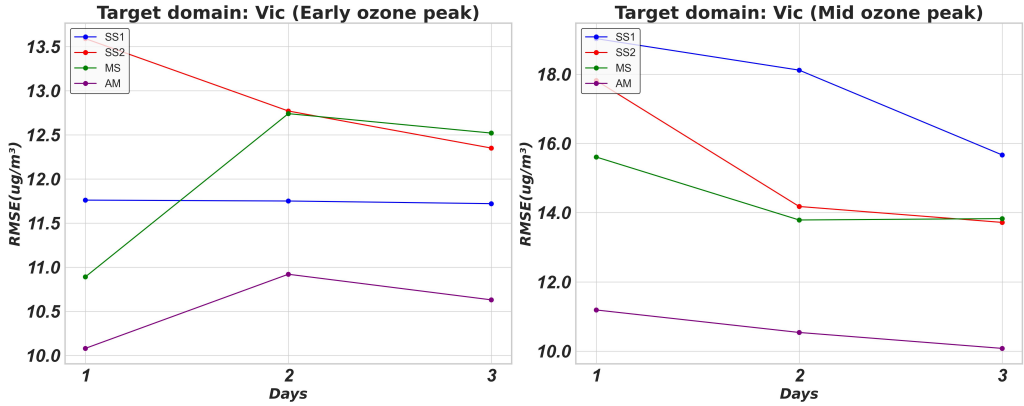

Fig. 5. Vic as target domain: RMSE comparison between the AM method and the three alternatives during the early and mid-phases of the ozone peak.

As observed in the figure, SS1 and SS2, which rely solely on co-location data from a single source domain, demonstrate instability in their performance. Specifically, while the SS1 method manifests decent performance during the initial phase of the ozone peak in Vic, it lags behind other methods during the middle phase. Conversely, the MS method, with its model pre-trained on data from two source domains, exhibits more consistent performance across both phases compared to SS1 and SS2.

Under the condition of using only one to three days' data from the target domain, Vic, the AM method's average RMSE significantly outperforms the other three methods during both the early and middle stages of the ozone peak. This superior performance can be attributed to the MAML approach, which effectively leverages data from both source domains and promptly adapts to the target domain.

Test results with Manlleu and Vic as the source domains, Tona as the target domain and Tona and Vic as the source domains, Manlleu as the target domain can be seen in the Table 4 and Table 5, respectively. They all show similar results as in Table 2, which proves the effectiveness and universality of our method. Figures 6 and 7 present the intuitive results for the RMSE

Table 4a. Metrics of various calibration methods evaluated over Manlleu as the target domain utilizing 1–3 days' data from the early-phase of the ozone peak.

Method	1 day			2 days			3 days		
	MAE	RMSE	R^2	MAE	RMSE	R^2	MAE	RMSE	R^2
UC	123.25	160.87	–13.64	123.86	161.15	–14.16	123.54	161.29	–14.28
TT	63.60	75.72	–2.24	62.61	74.00	–2.19	62.01	72.98	–2.12
SS1	8.99	11.98	0.92	9.50	12.62	0.91	10.23	13.72	0.89
SS2	9.45	12.88	0.91	9.68	13.21	0.90	10.64	14.34	0.88
MS	7.68	10.95	0.93	8.55	12.17	0.91	10.30	14.52	0.88
AM	6.53	8.69	0.96	9.89	13.06	0.90	8.76	11.31	0.93

Table 4b. Metrics of various calibration methods evaluated over Manlleu as the target domain utilizing 1–3 days' data from the mid-phase of the ozone peak.

Method	1 day			2 days			3 days		
	MAE	RMSE	R^2	MAE	RMSE	R^2	MAE	RMSE	R^2
UC	82.71	109.34	–6.44	81.29	107.45	–6.21	80.70	106.79	–6.29
TT	60.68	72.37	–2.25	59.01	70.62	–2.11	57.67	68.95	–2.03
SS1	8.50	10.74	0.93	9.16	11.61	0.92	9.22	11.44	0.92
SS2	9.68	12.40	0.90	9.72	12.32	0.91	9.39	11.85	0.91
MS	8.39	11.38	0.92	8.78	11.15	0.92	8.66	10.87	0.92
AM	8.44	10.44	0.93	8.20	10.73	0.93	8.65	11.15	0.92

Table 5a. Metrics of various calibration methods evaluated over Tona as the target domain utilizing 1–3 days' data from the early-phase of the ozone peak.

Method	1 day			2 days			3 days		
	MAE	RMSE	R^2	MAE	RMSE	R^2	MAE	RMSE	R^2
UC	178.82	201.49	–22.37	172.63	194.54	–20.39	165.53	184.96	–18.23
TT	84.71	94.30	–4.09	83.08	92.94	–3.85	82.87	92.57	–3.79
SS1	9.26	13.27	0.90	9.01	12.60	0.91	10.56	14.59	0.88
SS2	15.13	22.45	0.71	12.23	18.28	0.81	12.20	17.76	0.82
MS	11.60	16.76	0.84	9.90	14.28	0.89	10.00	14.16	0.89
AM	8.79	11.11	0.93	10.49	13.73	0.89	9.44	12.84	0.91

Table 5b. Metrics of various calibration methods evaluated over Tona as the target domain utilizing 1–3 days' data from the mid-phase of the ozone peak.

Method	1 day			2 days			3 days		
	MAE	RMSE	R^2	MAE	RMSE	R^2	MAE	RMSE	R^2
UC	118.69	135.87	14.14	120.28	137.24	–14.72	121.35	138.36	–15.17
TT	72.48	80.28	–4.30	71.37	78.78	–4.20	69.81	77.20	–4.05
SS1	10.48	13.13	0.86	13.71	16.89	0.76	12.80	15.99	0.78
SS2	10.26	12.81	0.87	10.61	13.48	0.85	9.84	12.75	0.86
MS	8.08	10.28	0.91	6.76	9.14	0.93	7.69	10.10	0.91
AM	6.54	8.99	0.93	6.75	9.26	0.93	6.51	8.70	0.94

performance metric from Tables 4 and 5, respectively, revealing findings analogous to those from Fig. 5. Moreover, considering the three figures collectively, our method AM proves superior to other compared methods in all test results across various times and locations when co-localization data is available for one day in the target domain. This underscores the fact that the MAML method, while ensuring stability and accuracy, adapts to new environments faster than the other methods.

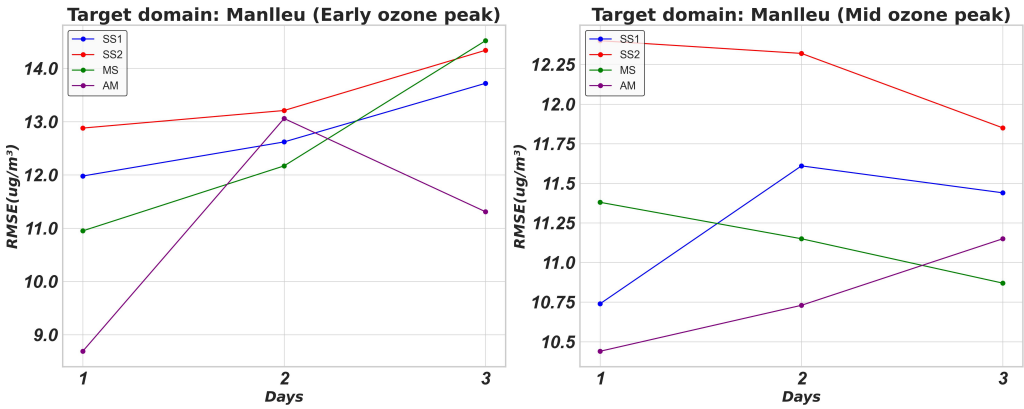

Fig. 6. Manlleu as the target domain: RMSE comparison between the AM method and three alternatives during the early and mid-phases of the ozone peak.

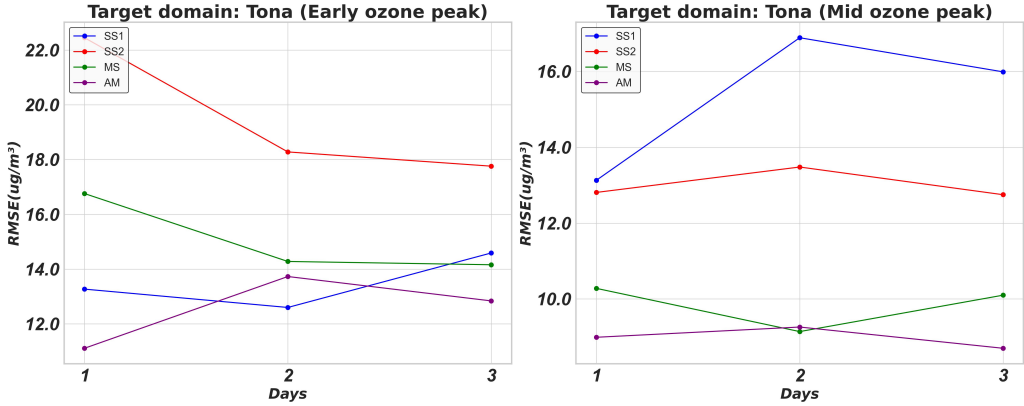

Fig. 7. Tona as target domain: RMSE comparison between the AM method and three alternatives during the early and mid-phases of the ozone peak.

Figures 8a and 8b show a comparison of the calibrated values and the reference station readings obtained from training and learning of our model using only one day of data in the target domain, respectively. (a) and (b) are for the early and mid-peak ozone in the Vic region, where the purple lines represent the calibrated LCSA output and the blue lines represent the ozone reference station readings.

Our method uses only one day's data in the target domain, and the resulting calibrated values perform well with the reference station readings in subsequent time periods because the self-attention module in ASCN takes into account the temporal pattern of ozone concentrations, and the inclusion of a shape distortion loss function further optimizes the trend of concentrations at spikes and troughs. The learning approach of MAML maximizes the use of data from the source domain. The learned parameters can be adapted for longer time periods in the future.

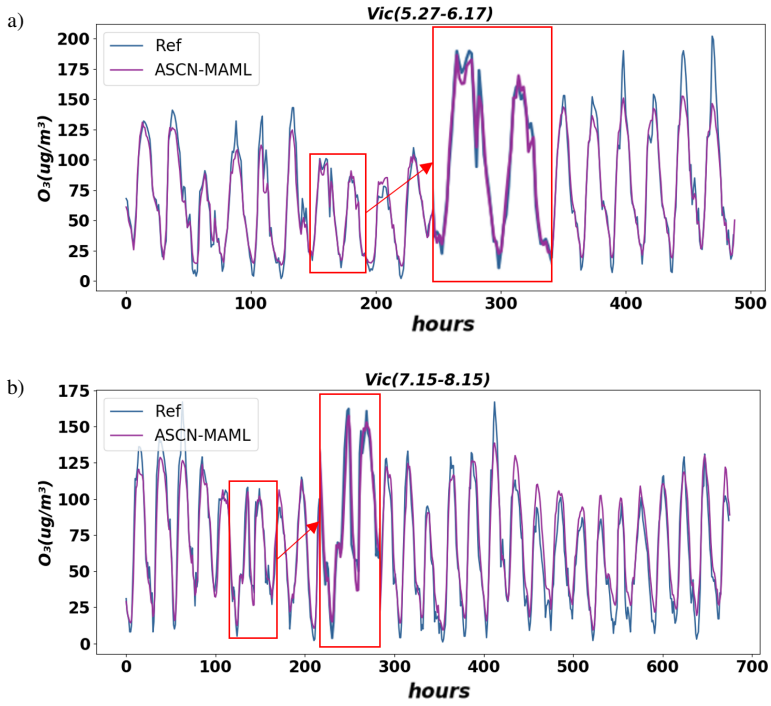

Fig. 8. Calibration results for the ASCN-MAML method: comparative analysis using one day's data from the Vic target domain for subsequent time periods. (a) early phase of the ozone peak (b) median phase of the ozone peak.

4. Conclusions

This paper proposes a low-cost ozone sensor array calibration method, ASCN-MAML, which addresses the problems of degraded cross-domain performance of calibration models and limited co-location time of reference stations in the target domain. The self-attention module and shape distortion loss function in the basic model of ASCN overcome the inability of other conventional models to capture the temporal patterns of ozone concentration variation and shape distortion at concentration spikes and troughs. The training approach using MAML, with the help of multiple source domain data, enables the model to learn the optimal parameters that can adapt to the full-time ozone concentration in the target domain. The test results from a real ozone dataset show that ASCN-MAML produces accurate calibration results over the following tens of days, both at the beginning and middle of the ozone peak, with the aid of 1–3 days of data from the target domain. Using Manlleu and Tona as source domains and Vic as the target domain, for example, our method compared to the original uncalibrated sensor readings showed an average reduction in MAE, RMSE of 66.95 and 87.26 and an average improvement in R2 from -5.44 to 0.93, compared to the next best result of the pre-trained-trimmed multi-source migration-based calibration method, with an average reduction in MAE, RMSE of 17.06% and 6.71%, and an average improvement in R2 of 4.21%. Our method enables the model to have high calibration accuracy and generalization capability under the condition that the calibration model is oriented to cross-domain and the target domain reference station data acquisition is limited, which can be effectively applied to practical ozone monitoring systems.

In the future, we will continue our in-depth research to further improve the stability and accuracy of our calibration models and expand their applicability to more types of gases, such as CO_2, CO, SO_2, formaldehyde, *etc*. At the same time, we will continue to explore more efficient calibration methods and deploy large-scale low-cost sensor arrays to support our conclusions with more data, to contribute to air quality monitoring and environmental protection. Moreover, we will further delve into the influence of drift caused by prolonged deployment of low-cost sensors on the precision of calibration models, seeking a calibration model that can maintain excellent accuracy even after long-term deployment.

Acknowledgements

We gratefully acknowledge the financial support provided by the China National Key R&D Program (2021YFF0600100) for our research. This support was essential in enabling our research to be conducted successfully.

References

[1] World Health Organization. (2022). *Ambient air pollution attributable deaths*. https://www.who.int/data/gho/data/indicators/indicator-details/GHO/ambient-air-pollution-attributable-deaths

[2] Alphasense Ltd. (2023). *Alphasense Application Note (AAN 110), Environmental changes: Temperature, pressure, humidity*. http://www.alphasense.com/WEB1213/wp-content/uploads/2013/07/AAN_110.pdf

[3] Lee, H., Kang, J., Kim, S., Im, Y., Yoo, S., & Lee, D. (2020). Long-term evaluation and calibration of low-cost particulate matter (PM) sensor. *Sensors*, *20*(13), 3617. https://doi.org/10.3390/s20133617

[4] Spinelle, L., Gerboles, M., Villani, M. G., Aleixandre, M., & Bonavitacola, F. (2015). Field calibration of a cluster of low-cost available sensors for air quality monitoring. Part A: Ozone and nitrogen dioxide. *Sensors and Actuators B: Chemical*, *215*, 249–257. https://doi.org/10.1016/j.snb.2015.03.031

[5] Christakis, I. G. H., Stavrakas, I., & Tsakiridis, O. (2020). Low cost sensor implementation and evaluation for measuring NO2 and O3 pollutants. *2020 9th International Conference on Modern Circuits and Systems Technologies (MOCAST), Bremen, Germany*, 1–4. https://doi.org/10.1109/MOCAST49295.2020.9200245

[6] Kang, Y., Aye, L., Ngo, T. D., & Zhou, J. (2022). Performance evaluation of low-cost air quality sensors: A review. *Science of the Total Environment*, *818*, 151769. https://doi.org/10.1016/j.scitotenv.2021.151769

[7] Morawska, L., Thai, P. K., Liu, X., Asumadu-Sakyi, A., Ayoko, G., Bartonova, A., Bedini, A., Chai, F., Christensen, B., & Dunbabin, M. (2018). Applications of low-cost sensing technologies for air quality monitoring and exposure assessment: How far have they gone? *Environment International*, *116*, 286–299. https://doi.org/10.1016/j.envint.2018.04.018

[8] Rai, A. C., Kumar, P., Pilla, F., Skouloudis, A. N., Di Sabatino, S., Ratti, C., Yasar, A., & Rickerby, D. (2017). End-user perspective of low-cost sensors for outdoor air pollution monitoring. *Science of the Total Environment*, *607*, 691–705. https://doi.org/10.1016/j.scitotenv.2017.06.266

[9] Eichstädt, S., Vedurmudi, A. P., Gruber, M., & Hutzschenreuter, D. (2022, September 19–21). *Fundamental aspects in data analysis for sensor network metrology*. IMEKO TC6 International Conference on Metrology and Digital Transformation, Berlin, Germany. https://doi.org/10.21014/actaimeko.v12i1.1417

[10] Christakis, I., Hloupis, G., Tsakiridis, O., & Stavrakas, I. (2022, 8–10 June 2022). *Integrated open source air quality monitoring platform*. 2022 11th International Conference on Modern Circuits and Systems Technologies (MOCAST), Bremen, Germany. https://doi.org/10.1109/MOCAST54814.2022.9837555

[11] Castell, N., Dauge, F. R., Schneider, P., Vogt, M., Lerner, U., Fishbain, B., Broday, D., & Bartonova, A. (2017). Can commercial low-cost sensor platforms contribute to air quality monitoring and exposure estimates? *Environment International*, *99*, 293–302. https://doi.org/10.1016/j.envint.2016.12.007

[12] Borrego, C., Costa, A. M., Ginja, J., Amorim, M., Coutinho, M., Karatzas, K., Sioumis, T., Katsifarakis, N., Konstantinidis, K., & De Vito, S. (2016). Assessment of air quality microsensors versus reference methods: The EuNetAir joint exercise. *Atmospheric Environment*, *147*, 246–263. https://doi.org/10.1016/j.atmosenv.2016.09.050

[13] Maag, B., Zhou, Z., & Thiele, L. (2018). A Survey on Sensor Calibration in Air Pollution Monitoring Deployments. *IEEE Internet of Things Journal*, *5*(6), 4857–4870. https://doi.org/10.1109/jiot.2018.2853660

[14] Narayana, M. V., Jalihal, D., & Nagendra, S. M. (2022). Establishing A Sustainable Low-Cost Air Quality Monitoring Setup: A Survey of the State-of-the-Art. *Sensors*, *22*(1), 394. https://doi.org/10.3390/Rs22010394

[15] Ferrer-Cid, P., Barcelo-Ordinas, J. M., Garcia-Vidal, J., Ripoll, A., & Viana, M. (2020). Multisensor Data Fusion Calibration in IoT Air Pollution Platforms. *IEEE Internet of Things Journal*, *7*(4), 3124–3132. https://doi.org/10.1109/jiot.2020.2965283

[16] Cordero, J. M., Borge, R., & Narros, A. (2018). Using statistical methods to carry out in field calibrations of low cost air quality sensors. *Sensors and Actuators B: Chemical*, *267*, 245–254. https://doi.org/10.1016/j.snb.2018.04.021

[17] Lin, Y., Dong, W., & Chen, Y. (2018). Calibrating Low-Cost Sensors by a Two-Phase Learning Approach for Urban Air Quality Measurement. *Proceedings of the ACM on Interactive, Mobile, Wearable and Ubiquitous Technologies*, *2*(1), 1–18. https://doi.org/10.1145/3191750

[18] Chattopadhyay, A., Huertas, A., Rebeiro-Hargrave, A., Fung, P. L., Varjonen, S., Hieta, T., Tarkoma, S., & Petaja, T. (2022). Low-Cost Formaldehyde Sensor Evaluation and Calibration in a Controlled Environment. *IEEE Sensors Journal*, *22*(12), 11791–11802. https://doi.org/10.1109/jsen.2022.3172864

[19] Christakis, I., Tsakiridis, O., Kandris, D., & Stavrakas, I. (2023). Air Pollution Monitoring via Wireless Sensor Networks: The Investigation and Correction of the Aging Behavior of Electrochemical Gaseous Pollutant Sensors. *Electronics*, *12*(8), 1842. https://www.mdpi.com/2079-9292/12/8/1842

[20] Cheng, Y., Saukh, O., & Thiele, L. (2022). SensorFormer: Efficient Many-to-Many Sensor Calibration With Learnable Input Subsampling. *IEEE Internet of Things Journal*, *9*(20), 20577–20589. https://doi.org/10.1109/jiot.2022.3177948

[21] Cheng, Y., Li, X., Li, Z., Jiang, S., Li, Y., Jia, J., & Jiang, X. (2014). *AirCloud: a cloud-based air-quality monitoring system for everyone*. Proceedings of the 12th ACM Conference on Embedded Network Sensor Systems, Memphis, Tennessee. https://doi.org/10.1145/2668332.2668346

[22] Yu, H., Li, Q., Wang, R., Chen, Z., Zhang, Y., Geng, Y-a., Zhang, L., Cui, H., & Zhang, K. (2020). A Deep Calibration Method for Low-Cost Air Monitoring Sensors with Multilevel Sequence Modeling. *IEEE Transactions on Instrumentation and Measurement*, *69*(9), 7167–7179. https://doi.org/10.1109/tim.2020.2978596

[23] Jha, S. K., Kumar, M., Arora, V., Tripathi, S. N., Motghare, V. M., Shingare, A. A., Rajput, K. A., & Kamble, S. (2021). Domain Adaptation-Based Deep Calibration of Low-Cost PM2.5 Sensors. *IEEE Sensors Journal*, *21*(22), 25941–25949. https://doi.org/10.1109/JSEN.2021.3118454

[24] Cheng, Y., He, X., Zhou, Z., & Thiele, L. (2019). ICT: In-field Calibration Transfer for Air Quality Sensor Deployments. *Proceedings of the ACM on Interactive, Mobile, Wearable and Ubiquitous Technologies*, *3*(1), 1–19. https://doi.org/10.1145/3314393

[25] Li, G., Ma, R., Liu, X., Wang, Y., & Zhang, L. (2020). *RCH: robust calibration based on historical data for low-cost air quality sensor deployments*. Adjunct Proceedings of the 2020 ACM International Joint Conference on Pervasive and Ubiquitous Computing and Proceedings of the 2020 ACM International Symposium on Wearable Computers, Virtual Event, Mexico. https://doi.org/10.1145/3410530.3414322

[26] Robin, Y., Amann, J., Goodarzi, P., Schütze, A., & Bur, C. (2022). Transfer Learning to Significantly Reduce the Calibration Time of MOS Gas Sensors. 2022 IEEE International Symposium on Olfaction and Electronic Nose (ISOEN), Aveiro, Portugal. https://doi.org/10.1109/ISOEN54820.2022.9789596

[27] Yadav, K., Arora, V., Kumar, M., Tripathi, S. N., Motghare, V. M., & Rajput, K. A. (2022). Few-Shot Calibration of Low-Cost Air Pollution (PM2.5) Sensors Using Meta Learning. *IEEE Sensors Letters*, *6*(5), 1–4. https://doi.org/10.1109/LSENS.2022.3168291

[28] Vaswani, A., Shazeer, N., Parmar, N., Uszkoreit, J., Jones, L., Gomez, A. N., Kaiser, Ł., & Polosukhin, I. (2017). *Attention is all you need*. Proceedings of the 31st International Conference on Neural Information Processing Systems, Long Beach, California, USA. https://proceedings.neurips.cc/paper_files/paper/2017/hash/3f5ee243547dee91fbd053c1c4a845aa-Abstract.html

[29] He, P., Liu, X., Gao, J., & Chen, W. (2017). *DeBERTa: Decoding-enhanced BERT with disentangled attention*. International Conference on Learning Representations, Toulon. https://arxiv.org/abs/2006.03654

[30] Raffel, C., Shazeer, N., Roberts, A., Lee, K., Narang, S., Matena, M., Zhou, Y., Li, W., & Liu, P. J. (2020). Exploring the limits of transfer learning with a unified text-to-text transformer. *Journal of Machine Learning Research*, *21*(1), 5485–5551.

[31] Beltagy, I., Peters, M. E., & Cohan, A. (2020). *Longformer: The long-document transformer*. https://arxiv.org/abs/2004.05150

[32] Wu, S., Xiao, X., Ding, Q., Zhao, P., Wei, Y., & Huang, J. (2020). *Adversarial sparse transformer for time series forecasting*. Proceedings of the 34th International Conference on Neural Information Processing Systems, Vancouver, BC, Canada.

[33] Drouin, A., Marcotte, É., & Chapados, N. (2022). *Tactis: Transformer-attentional copulas for time series*. International Conference on Machine Learning, Hangzhou, China. https://proceedings.mlr.press/v162/drouin22a.html

[34] Guen, V. L., & Thome, N. (2019). *Shape and time distortion loss for training deep time series forecasting models*. Proceedings of the 33rd International Conference on Neural Information Processing Systems, Vancouver, Canada. https://proceedings.neurips.cc/paper_files/paper/2019/file/466accbac9a66b805ba50e42ad715740-Paper.pdf

[35] Finn, C., Abbeel, P., & Levine, S. (2017). *Model-Agnostic Meta-Learning for Fast Adaptation of Deep Networks*. Proceedings of the 34th International Conference on Machine Learning, Australia. https://proceedings.mlr.press/v70/finn17a.html

[36] Parnami, A., & Lee, M. (2022). *Learning from few examples: A summary of approaches to few-shot learning*. https://arxiv.org/abs/2203.04291

[37] Barcelo-Ordinas, J. M., Ferrer-Cid, P., Garcia-Vidal, J., Viana, M., & Ripoll, A. (2021). H2020 project CAPTOR dataset: Raw data collected by low-cost MOX ozone sensors in a real air pollution monitoring network. *Data in Brief*, *36*, 107127. https://doi.org/10.1016/j.dib.2021.107127

[38] Catalunya, G. D. (2023). *Vols saber que respires? Medi Ambient*. (in Catalan) http://mediambient.gencat.cat/es/05_ambits_dactuacio/atmosfera/qualitat_de_laire/vols-saber-que-respires/

[39] Lai, G., Chang, W.-C., Yang, Y., & Liu, H. (2018). *Modeling Long- and Short-Term Temporal Patterns with Deep Neural Networks*. The 41st International ACM SIGIR Conference on Research & Development in Information Retrieval, Ann Arbor, MI, USA. https://doi.org/10.1145/3209978.3210006

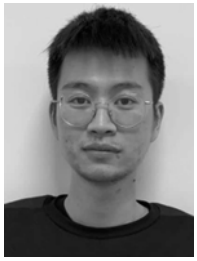

Tianliang Feng is a master's student at the College of Optics and Electronic Technology, China Jiliang University. His research focuses on the study of gas sensor networks and calibration algorithms.

Shangzhong Jin obtained his Ph.D. degree from Zhejiang University and is a professor in the College of Optics and Electronic Technology, China Jiliang University. His research interests include optics, spectroscopy, instrumentation, and metrology.

Xingchuang Xiong is a researcher at the National Institute of Metrology. His research area is the digital transformation of metrology.